HHS Public Access

Author manuscript

Cell Rep. Author manuscript; available in PMC 2019 January 15.

Published in final edited form as:

Cell Rep. 2017 December 12; 21(11): 3049–3064. doi:10.1016/j.celrep.2017.11.044.

Strict independence of parallel and poly-synaptic axon-target matching during visual reflex circuit assembly

Tania A. Seabrook[1], **Onkar S. Dhande**[1], **Nao Ishiko**[1], **Victoria P. Wooley**[1], **Phong L. Nguyen**[1], and **Andrew D. Huberman**[1,2,3,4,*]

[1]Department of Neurobiology, Stanford University School of Medicine, Stanford, CA 94304, USA

[2]Department of Ophthalmology, Stanford University School of Medicine, Palo Alto, CA 94303, USA

[3]Bio-X, Stanford University, Stanford University, CA 94305, USA

SUMMARY

The use of sensory information to drive specific behaviors relies on circuits spanning long distances that wire up through a range of axon-target recognition events. Mechanisms assembling poly-synaptic circuits and the extent to which parallel pathways can 'cross-wire' to compensate for loss of one another, remain unclear and are crucial to our understanding of brain development and models of regeneration. In the visual system, specific retinal ganglion cells (RGCs) project to designated midbrain targets connected to downstream circuits driving visuomotor reflexes. Here we deleted RGCs connecting to pupillary light reflex (PLR) midbrain targets, and discovered that axon-target matching is tightly regulated. RGC axons of the eye-reflex pathway avoided vacated PLR targets. Moreover, downstream PLR circuitry is maintained; hindbrain and peripheral components retained their proper connectivity and function. These findings point to a model in which poly-synaptic circuit development reflects independent, highly stringent wiring of each parallel pathway and downstream station.

Graphical abstract

[*]Correspondence: adh1@stanford.edu.
[4]Lead Contact

AUTHOR CONTRIBUTIONS

T.A.S. and A.D.H. conceived and designed the experiments and wrote the manuscript, T.A.S., N.I., and P.L.N. conducted behavior experiments, T.A.S., O.S.D., N.I., V.P.W., and P.L.N. performed histology, T.A.S. and V.P.W. imaged data, and T.A.S. performed all injections, analyzed data and assembled the manuscript.

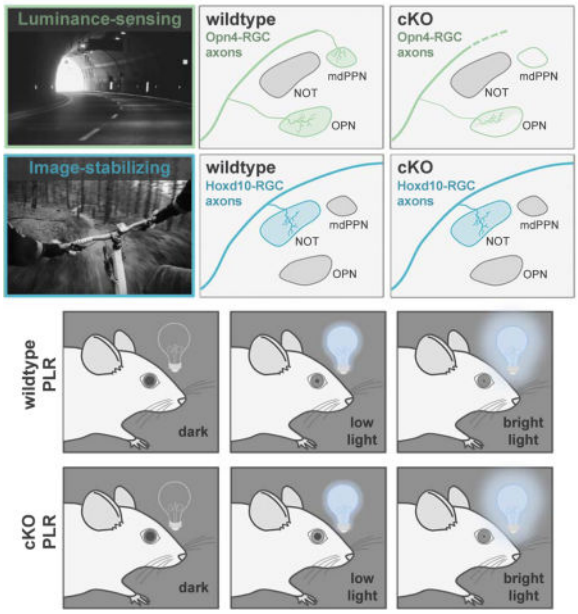

INTRODUCTION

Many of our sensations reliably drive specific adaptive behaviors, such as pain-avoidance reflexes (Fields and Heinricher, 1989; Abraira and Ginty et al., 2013; Han and Dong, 2014), fear-driven freezing and escape (Kobayakawa et al., 2007; Stowers et al., 2013; Yilmaz and Meister, 2013; Zhao et al., 2014; De Franceschi et al., 2016), and reproductive and social interactions (Anderson, 2016; Hashikawa et al., 2016; Stowers and Liberles, 2016; Yang and Shah, 2016). These behaviors emerge from sequential activation of synaptic stations positioned from the sensory periphery to the neuromuscular junction (Figure 1A) (Clark et al., 2013). Moreover, many of these nodes sort and combine different qualities of sensory information in parallel in order to correctly drive downstream targets (Figure 1B) (Luo and Flanagan, 2007).

What are the developmental steps that direct poly-synaptic parallel circuit assembly? Much has been learned about how axons pathfind to their targets and sort into maps within those targets (O'Leary et al., 1999; Huberman et al. 2008a; Bonanomi and Pfaff, 2010; Cang and Feldheim, 2013; Erskine and Herrera, 2014). This multistep process involves axon outgrowth (Sretavan, 1990; Polleux and Snider, 2010), steering through intermediate choice points (Schneider and Granato, 2003; Williams et al., 2004), target recognition and synapse formation, as well as the removal of projections and synaptic connections made with incorrect targets (Sanes and Yamagata, 2009; Huberman et al. 2008a; Riccomagno and Kolodkin, 2015). Genetically programmed molecular cues play integral roles in these processes (Dodd and Jessell, 1988; Raper and Mason, 2010; Kolodkin and Tessier-Lavigne, 2011) and neural activity sculpts and refines them (Huberman et al., 2008a). How functionally-precise parallel pathways emerge and the consequences of disrupting parallel wiring on downstream circuitry in the mammalian brain, remain poorly understood.

In recent years, the combination of Cre-drivers for specific neuronal populations in mice (Gong et al., 2007) and tools for manipulating the activity of Cre-expressing neurons (Fenno et al., 2011; Madisen et al., 2012; Urban and Roth, 2015; Whissell et al. 2016) has broadened understanding of how functionally specialized neurons in the sensory periphery lead to adaptive, defined patterns of motor outputs (Rossignol et al., 2006; Davidson and Giesler, 2010; Chen et al., 2011; Schmidt et al., 2011; Arber, 2012; Abraira and Ginty, 2013; Anderson 2016). With those functional reflex architectures now understood, such circuitries provide a rich opportunity to probe the principles and mechanisms of poly-synaptic network assembly and thereby fill a key gap in our understanding of mammalian brain development.

A longstanding model of parallel pathway assembly in the CNS is the visual system eye-to-brain (retinofugal) pathway (Shatz and Sretavan, 1986; Osterhout et al., 2014; Dhande et al., 2015; Seabrook et al., 2017; Zhang et al., 2017). Retinofugal circuits include ~30 types of retinal ganglion cells (RGCs), the output neurons of the eye that collectively project to ~40 different subcortical targets (Morin and Studholme, 2014), which in turn connect to downstream targets to create perceptions and drive visually-evoked behaviors (Dhande and Huberman, 2014; Dhande et al., 2015; Seabrook et al., 2017). Indeed, several visual channels are wired such that they reliably and robustly drive adaptive motor functions. Two primary examples of this are reflexive eye movements that occur when the head or eyes move (Simpson, 1984; Dhande et al., 2013) and the pupillary light reflex (PLR) in which the pupil or ‘aperture’ of the eye changes in response to shifts in overall ambient illumination (Güler et al., 2008; Hatori et al., 2008; Chen et al., 2011) (Figure 1F–1G). Both of these visuomotor reflexes are driven by specific RGC types that project to distinct targets in the midbrain pretectum (Figure 1B), which connect to more distal brainstem nuclei to engage cranial motor nuclei (Gamlin 2006; Schmidt et al., 2011; Dhande and Huberman, 2014; Dhande et al., 2015).

The poly-synaptic circuitry underlying both PLR and reflexive eye movements are becoming clear. In terms of PLR, intrinsically photosensitive RGCs (ipRGCs) project to the olivary pretectal nucleus (OPN) and medial posterior pretectal nucleus (mdPPN) (Figure 1B–1C). OPN activates downstream circuits including Edinger-Westphal nucleus (EW) to constrict iris muscles in response to increased illumination (Figure 1F–1G) (Lucas et al., 2003; Gamlin 2006; Güler et al., 2008; Hatori et al., 2008; Chen et al., 2011; Schmidt et al., 2011). The circuitry for reflexive eye movements, by contrast, involves a different RGC population, the slow-tuned direction-selective RGCs (slow-DSGCs). Slow-DSGCs innervate the nucleus of the optic tract (NOT) (Figure 1B), which connects via the brainstem and cerebellum, to control horizontal optokinetic nystagmus important for gaze stabilization (Simpson, 1984; Gamlin, 2006; Yonehara et al., 2009; Dhande et al., 2013; 2015; Dhande and Huberman, 2014).

Based on their close positioning, high degree of axon-target specificity across multiple synapses, and defined, highly quantifiable behavioral outputs, these two circuits carry many of the qualities essential for probing development of parallel pathway assembly and for understanding how downstream circuits are impacted by disruptions of different nodes along each pathway. Moreover, the timing of PLR and eye movement circuitry is offset in a manner that makes them ideal for exploring their influence on each other during

development. As a general population, RGCs in the mouse are born between embryonic day (E) 10 and postnatal day (P) 0 (Dräger, 1985; Hufnagel et al., 2010; Osterhout et al., 2014). Previous work revealed that the axons of the RGCs that target the OPN and are selectively labeled by a Cdh3-GFP transgenic mouse line (Osterhout et al., 2011) reach the OPN and mdPPN by E16, making them among the earliest group of RGCs to project to the brain. By contrast, the axons of the RGCs that drive eye reflexes first reach their brain targets at P7 (Osterhout et al., 2014).

Here we used Cre-dependent deletion of Tbr2, a transcription factor critical for RGC survival (Mao et al., 2008; 2014; Sweeney et al., 2014), to specifically eliminate the early-projecting cohort of luminance-sensing RGCs that connect to PLR centers in the visual brainstem (Figure 1C–1E). We find that even when OPN and mdPPN are rendered devoid of their normal retinal input, the axons of slow-DSGCs destined for eye movement centers continue to avoid PLR targets. Using circuit tracing and site-specific chemogenetic manipulations, we also find that the PLR pathway retains overall function even in the absence of sensory input indicating that wiring of subsequent nodes in sensory-reflex arcs are preserved.

RESULTS

A mouse line for manipulating luminance-sensing RGCs and circuits

To begin to address how parallel visual inputs to brainstem wire up, interact and impact downstream pathways, we sought mouse lines to selectively target and manipulate luminance-sensing RGCs. We screened a library of transgenic BAC-Cre recombinase driver lines (GENSAT; Gong et al., 2007) and identified the tryptophan hydroxylase 2 Cre mouse line ($Tph2^{Cre}$) as a possible candidate. To characterize the $Tph2^{Cre}$ mice, we crossed them with a reporter line expressing tdTomato and examined the eyes and brains of their offspring (Figure 2A). Within retina, $Tph2^{Cre}$-tdTomato expression was found mainly in the ganglion cell layer (GCL) and was present as early as E14.5 (Figure 2B–2I). We applied immunostaining with the RGC specific marker, RBPMS (Rodriguez et al., 2014), and confirmed that 98% (n = 3 mice) of $Tph2^{Cre}$ cells in the GCL were indeed RGCs as opposed to displaced amacrine cells, the other major cell population in this retinal layer (Figure 2J–2L).

Next we crossed $Tph2^{Cre}$-tdTomato mice with Cdh3-GFP mice to generate $Tph2^{Cre}$-tdTomato;Cdh3-GFP offspring. Cdh3-GFP RGCs (hereafter ‘Cdh3-RGCs’) are made up of M2 ipRGCs and ‘diving’ RGCs. Both populations are found in the ventral two-thirds of the retina and target OPN, the pretectal target involved in PLR (Osterhout et al., 2011). Cdh3-RGCs are among the earliest born RGCs and the first to send their axons from the eye into the brain (Osterhout et al., 2014). Immunostaining revealed that 90% (n = 4 mice) of Cdh3-RGCs express $Tph2^{Cre}$ (Figure 2M–2O) and that 84% (n = 3 mice) of melanopsin^{+} RGCs express $Tph2^{Cre}$ (Figure 2P–2R).

Subsequently, we examined the patterns of axonal projections from $Tph2^{Cre}$-tdTomato RGCs to retinorecipient regions of the brain including the dorsal midbrain pretectum. We injected an anterograde tracer, cholera toxin subunit B conjugated to Alexa 488 (CTb-488;

green), into both eyes of Tph2^{Cre}-tdTomato mice in order to visualize the axons of all RGCs and their retinorecipient terminations (Figure 2S) (Morin and Studholme, 2014). We then analyzed which CTb^{+} retinorecipient regions also contained tdTomato^{+} axons (n = 5 mice). In the pretectal region of the dorsal midbrain, Tph2^{Cre} RGC axons innervated the OPN and mdPPN but were not seen in the NOT (Figure 2T–2Y) an intervening target that receives input from slow-DSGCs and is involved in generating horizontal slip-compensating eye movements (Dhande et al., 2013). Together these results demonstrate that Tph2^{Cre} marks luminance-sensing RGCs projecting to the OPN and mdPPN but not image-stabilizing RGCs that project to nearby visual targets. Thus Tph2^{Cre} mice allow for labeling and manipulation of a select population of RGCs whose axons undergo highly specific patterns of targeting in the brain pretectum, making this an attractive tool for probing various aspects of axon-target matching in the developing visual system.

Tbr2 is a transcriptional regulator of survival expressed by luminance-sensing RGCs

Competition plays a critical role in development of mammalian eye-specific and retinotopic maps (reviewed in Huberman et al., 2008a; Cang and Feldheim, 2013; Seabrook et al., 2017) and in the development of neuromuscular connections (Sanes and Lichtman, 1999; Bonanomi and Pfaff, 2010), but it plays a more limited role in cell-cell specific wiring in the spinal cord (Betley et al., 2009). We sought to understand whether, at the level of axon-whole target matching in the visual brainstem, specific RGC types undergo competition to arrive at their final pattern of parallel connectivity. Typically, competition occurs within a target where axons of various cell types overlap or converge during development. Although the different RGC subtypes innervating pretectum go to discrete targets, they traverse through a common region to reach those targets. Thus, removal of one subtype may influence the targeting of other RGC axons. In order to test this, we sought to eliminate luminance-sensing RGCs at a time before other RGC types begin to innervate the brain. The T-box transcription factor Tbr2 (also known as Eomes) is critical for the survival of a subpopulation of RGCs (Mao et al., 2008; 2014; Sweeney et al., 2014). Like Tph2^{Cre}, Tbr2 is expressed mainly in the GCL and turns on early in ganglion cell genesis, at ~E14 (Mao et al., 2008). Our rationale was that if Tbr2 is present in luminance-sensing RGCs but not other RGC types, then removing Tbr2 would lead to an early loss of RGCs projecting to the OPN and mdPPN.

We immunostained retinas for Tbr2 in various lines of transgenic mice that each have GFP in different subtypes of RGCs (Figure 3A–3R) (Dhande et al., 2015) and found that Tbr2 was highly expressed by luminance-sensing RGCs labeled in Cdh3-GFP (Figure 3A–3C and 3S) and Opn4-GFP mice (Figure 3D–3F and 3S). By contrast, we observed little or no expression of Tbr2 in other RGC types (Figure 3G–3R and 3S). A small percentage (9%) of slow-DSGCs, labeled by Hoxd10-GFP, did express Tbr2, however because < 3% of Hoxd10-RGCs expressed both Tbr2 and Tph2^{Cre} (Figure S1) those cells are not vulnerable to Cre-dependent manipulations of the sort we describe here and thus should have a minimal effect on RGCs important for image stabilization. Tbr2 was not found in any retinorecipient subcortical nuclei (Figure S2; see also Sweeney et al. 2014) and thus the consequences of our genetic manipulation should be of retinal origin.

The overlap between Tbr2 and Tph2^{Cre} in RGCs was substantial (Figure 3T–3W). Immunostaining confirmed that whereas Tbr2^{+} RGCs made up only approximately a quarter of the total Tph2^{Cre} population (Figure 3Y), the vast majority (82%) of Tbr2^{+} RGCs expressed Tph2^{Cre} (Figure 3X). The expression of both Tbr2 and Tph2^{Cre} in nearly all luminance-sensing RGCs (Figure 3Z) raised the opportunity to exploit the requirement of Tbr2 for neuronal survival to selectively ablate retinal input to the OPN and mdPPN early in development and thereby explore the impact of that removal on targeting of slow-DSGCs and that normally target nearby regions of brainstem.

Conditional deletion of Tbr2 in luminance-sensing RGCs causes early depletion of their axon projections to the visual brainstem

To assess the impact of conditionally removing Tbr2 from Tph2^{Cre} cells, we generated Tbr2$^{fl/fl}$;Tph2^{Cre};Cdh3-GFP (cKO) mice (Figure 4A). Examination of retinas revealed a near complete loss of Cdh3-RGCs compared to littermate controls (wildtype) (Figure 4B–4C). Next we labeled all RGC axons using CTb-594 (magenta) and examined the CTb^{+} retinorecipient zones in the brainstem for the presence of Cdh3-RGC axons (green) in cKO and control mice at P20 – a stage after retinofugal wiring and axon-target specificity is completed (Osterhout et al., 2014) (Figure 4D–4O). Whereas normal inputs to the OPN and mdPPN were present in all control mice (Figure 4E and 4K) (Osterhout et al., 2011; 2014), in cKOs the OPN (Figure 4H) and mdPPN (Figure 4N) were notably devoid of axons from Cdh3-RGCs (schematized in Figure 4Q). Measurements of the percentage of target space innervated by Cdh3-RGC axons confirmed that conditional removal of Tbr2 from Tph2^{Cre} RGCs resulted in a significant loss of GFP^{+} axon terminal fields in both OPN and mdPPN (Figure 4P). A very sparse pattern of retinal innervation was seen in the OPN of some mice but the vast majority of RGC inputs to OPN (~80%) were ablated (Figure 4G, schematized in Figure 4Q).

The absence of Cdh3-RGC axons connecting to the OPN and mdPPN in cKO mice on P20 does not necessarily indicate that Cdh3-RGC axons failed to *ever* reach those targets. To further explore how this phenotype arose, we examined Cdh3-RGC innervation at an earlier age, P7, in both the cKO mice and their wildtype littermates (Figure S3). Similar to the phenotype observed at P20, Cdh3-RGC axons were missing from the OPN and mdPPN of cKO mice (Figure S3A–S3F and S3M–S3R). Additionally, whereas Cdh3-RGC axons transiently project to the superior colliculus (SC) in controls (Osterhout et al., 2011; 2014), such projections were absent from cKOs at this age (Figure S3S–S3X). Cdh3-RGC axons were observed in the medial terminal nucleus (MTN) of both wildtype and cKO mice at P7 (s) - an age when they typically project to and then later withdraw from this target (Osterhout et al., 2014). These findings indicate that Tbr2 conditional mutations can be used to delete specific sets of Cre-expressing RGCs; in this case, specifically the RGCs that project to the midbrain nuclei controlling PLR. Moreover, this ablation is achieved prior to when a different population of RGCs- the image-stabilizing slow-DSGCs, are just beginning to innervate adjacent targets in pretectum (Osterhout et al., 2014).

Lack of cross-wiring among parallel retinofugal pathways to brainstem

Connections between slow-DSGCs and the NOT form part of the accessory optic system (AOS) and play a critical role in maintaining stable visual perception during movement. Slow-DSGCs encoding for forward motion, are labeled in the Hoxd10-GFP line (Dhande et al., 2013), project to the NOT and are important for generating reflexive horizontal eye movements to compensate for retinal slip (Dhande et al., 2015; Osterhout et al., 2015). The NOT resides directly between OPN and mdPPN and slow-DSGCs that innervate NOT arrive well after Cdh3-RGCs innervate their targets (Osterhout et al., 2014). Thus, we tested whether vacating the targets of early-innervating Cdh3-RGCs enables the later-arriving Hoxd10-RGCs to enter and form connections with OPN and mdPPN as a direct test of the extent to which parallel retinofugal pathways can 'cross-wire' in each others' absence.

We examined CTb-labeled RGC axons (magenta) and Hoxd10-RGC axons (cyan) in cKOs and wildtype littermates on P20 (Figure 5). In cKOs, GFP^+ axons continued to avoid the OPN (Figure 5E) and mdPPN (Figure 5Q) (schematized in Figure 5T). Moreover, innervation of their normal targets, NOT and MTN, appeared undisrupted (Figure 5K and 5Q). No significant change in the innervation pattern of Hoxd10-RGCs was found in cKO mice when compared to wildtype (Figure 5S).

In theory, Hoxd10-RGC axons could have entered the OPN and mdPPN early and then retracted their axons from these targets before the time we initially studied. Therefore, we looked at their projection pattern in cKO mice, in the first postnatal week (P5–P8), when these RGCs begin to innervate pretectum (Figure S4). Again, they were absent from OPN (Figure S4E) and mdPPN (Figure S4Q) and no significant differences in the percent of retinorecipient targets innervated by Hoxd10-RGC axons were found (Figure S4S).

Apparently, regardless of whether or not the OPN and mdPPN are occupied by luminance-sensing RGC axons, slow-DSGC axons that enter this general region still avoid these targets (Figure 5 and S4). However, all RGCs traverse through the retinofugal pathway together which led us to explore for potential impacts on other RGC types. We next examined projections from the posterior-tuned On-Off DSGCs expressing TRHR-GFP in cKO mice (Figure S5). TRHR-RGCs form part of image-forming pathway; their main targets are the dorsal lateral geniculate nucleus (dLGN) shell and SC (Huberman et al., 2009; Rivlin-Etzion et al., 2011). Analogous to Hoxd10-RGCs, the TRHR-RGCs begin entering their targets after the first postnatal week while coursing past the OPN and mdPPN (Osterhout et al., 2014). In cKOs, these DSGCs did not enter OPN (Figure S5K) or mdPPN (Figure S5Q), similar to slow-DSGCs. TRHR-RGCs maintained their normal projections to the shell of dLGN (Figure S5) and the SC (Figure S5T) in cKO mice (Figure S5E and S5W) (Figure S5Y). Taken together, these results reveal that even if the OPN and mdPPN lack their typical input from luminance-sensing RGCs, other RGC types continue to avoid these nuclei. This suggests that availability of target space is not a key factor in guiding the axon-target matching process in pretectum.

A subset of ipRGCs escapes Tph2^{Cre}-mediated genetic ablation

Visualization of all RGC axons indicated that some remain present in the OPN of cKO mice, but which RGC type do they originate from? Cdh3-GFP only labels a subset of RGCs projecting to the OPN, therefore we used the Opn4-GFP mouse line, which marks all luminance-sensing RGCs, to see whether any of these cells were spared by the Cre-mediated ablation (Figure 6A–6M and S6). Indeed we found that although there were very few, Opn4-RGC axons were present in the OPN of cKOs (Figure 6E and 6K). To further confirm that the retinal input in cKO mice is from spared ipRGCs, we injected a glycoprotein-deleted modified rabies virus encoding mCherry (ΔG-RABV-mCherry) into OPN to retrogradely infect RGCs and found that these RGCs express Opn4-GFP (Figure S6, n = 2 out of 2 RGCs). Although nearly all Opn4-RGCs express Tbr2 (Figure 3D–3F and 3S), approximately 15% of luminance-sensing RGCs did not have Tph2^{Cre} (Figure 2P–2R). Thus, Tbr2 would not be deleted in the cells lacking Cre and consequently would evade genetic ablation.

Effects of ablating luminance-sensing RGCs on the poly-synaptic PLR circuit

What changes might occur along the PLR circuit (Figure 1F) to compensate for the lack of retinal input? To begin to investigate whether there are any affects on postsynaptic cells in OPN, we first stained for parvalbumin (PV), a marker for a population of OPN cells (Prichard et al., 2002; Osterhout et al., 2011), in wildtype and cKO mice (Figure 6N–6S). We found that there was a significant decrease in the number of PV^{+} cells in cKOs (Figure 6R and 6T). This suggests that loss of retinal input leads to either a reduction in PV expression in OPN or alternatively could indicate neuronal loss in this nucleus. To determine if the latter occurred, we examined the number of cells in OPN of wildtype and cKO mice using the fluorescent Nissl stain, NeuroTrace (Figure S7). The reduction in PV expression in the OPN was not due to loss of these cells as there was no difference in overall cell number in cKOs compared to littermate controls (Figure S7I).

Since the connections between OPN and EW are crucial downstream connections for driving PLR, we next examined the OPN cells that are directly connected to EW via retrograde tracing (Figure 6U–6CC). Injection of ΔG-RABV into EW (Figure 6U, 6V and 6Z) retrogradely labeled cells in the OPN of both cKOs (Figure 6W–6Y) and littermate controls (Figure 6AA–6CC). These results indicate there may be cellular changes occurring within the OPN following the loss of sensory input but the output neurons and their connections to EW are intact.

The remaining PLR pathway functions normally in the absence of sensory input

One of the main functions of the OPN and its connections is to generate the PLR or contraction of sphincter pupillae muscle in the iris which reduces pupil size to compensate for increases in illumination (Figure 1F) (Gamlin 2006). This prevents image saturation as well as adjusts the depth of field to see sharply across a wide range of distances (Figure 1G) (Campbell and Gregory, 1960; Do et al. 2010). We observed a near complete loss (~80%) of the typical input to OPN in cKOs that was not compensated for by other RGC types. How does this affect the functional output of the PLR circuit? To assess this we recorded and measured pupil size of wildtype and cKO mice from when the pupil was fully dilated after

dark adaption (baseline), during stimulation with light (470 nm) within the peak spectral sensitivity of melanopsin (constriction), and post-illumination (relaxation) (Figure 7A–7I). At low (Figure 7A–7C) and moderate (Figure 7D–7F) light intensities pupil constriction was significantly attenuated in cKOs compared to controls. However, at high light intensity, PLR was not altered in cKO mice (Figure 7G–7I). During light stimulation, the pupil of cKOs reached and maintained a peak constriction equivalent to wildtype (Figure 7G–7I). The major loss of retinal input to OPN following Cre-dependent deletion of Tbr2 produces weakened constriction of the pupil in response to light at low to moderate intensities, however, high levels of light can counteract the deficit to retinal input and generate a normal PLR response.

Chemogenetic activation of the neurons along the PLR pathway leads to pupil constriction

Our PLR experiments using high intensity light demonstrated that this type of intense stimulation is sufficient to drive the circuit to produce a normal pupil constriction (Figure 7G–7I). In order to drive cells at different stations along the PLR pathway, we turned to the use of chemogenetic tools employing designer receptors exclusively activated by designer drugs (DREADDs) (Urban and Roth, 2015). The DREADD, human M3 muscarinic designer receptor (hM3D) can be expressed in cells through an adeno-associated virus (AAV) delivery system and exposure of this receptor to the synthetic ligand clozapine-*N*-oxide (CNO) activates its G_q-mediated signaling leading to neuronal excitation (Figure 7J). Previously, our lab revealed that bath application of CNO during *in vitro* whole-cell recordings from RGCs infected with hM3D leads to a drastic increase in spike firing of these cells (Lim et al., 2016). Moreover, peripheral administration of CNO can produce behavioral effects for up to 6 hours (Whissell et al., 2016).

First we tested whether pupil constriction could be induced in the absence of light by chemogenetically activating either $Tph2^{Cre}$ RGCs (Figure 7L) or a random RGC population (Figure 7M). We infected RGCs through intravitreal injection of AAVs to express either Cre-dependent (Figure 7L) or non-Cre-dependent (Figure 7M) hM3D. Several weeks later, the pupils of these mice were recorded in the dark pre- and post-CNO injection (Figure 7K). Injection of CNO should produce a chemogenetic driven PLR in darkness through activation of retinal cells expressing hM3D and we did indeed see this in wildtype animals (Figure 7L–7M). However, activation of $Tph2^{Cre}$ RGCs expressing Cre-dependent hM3D in cKO mice produced little or no pupil constriction (Figure 7L), which was expected due to the loss of Cre-expressing RGCs that project to OPN (see Figure 4). Conversely, when a non-Cre-dependent hM3D was used, pupil constriction was observed in the dark following CNO injection in both wildtype and cKO mice (Figure 7M). Most likely in cKOs, injection of CNO activates spared ipRGCs (see Figure 6) infected with the non-Cre-dependent hM3D.

Next we wanted to directly activate postsynaptic neurons of luminance-sensing RGCs in OPN to further test function along the PLR pathway. We bilaterally injected an AAV into the OPN in both hemispheres to express non-Cre-dependent hM3D (Figure 7N). When OPN neurons expressing hM3D were activated by injection of CNO, constriction of the pupil was observed in darkness in both wildtype and cKO mice (Figure 7N). The amount of pupil constriction in cKOs was significantly larger than that seen in controls (Figure 7N). One

possibility is that this reflects compensatory changes to diminished sensory input such as increased excitability of OPN neurons in cKOs. Together these results show that strong, direct stimulation of spared luminance-sensing RGCs or OPN neurons leads to pupil constriction in cKO mice. Even with reduced sensory input, PLR circuits seem to retain their appropriate connectivity and function, suggesting that the neurons and their circuits downstream of luminance-sensing RGCs develop independently of their RGC input.

DISCUSSION

Here we examined how parallel poly-synaptic circuits develop in the mammalian visual system. By focusing on two distinct sets of retinal output circuits that each target the brainstem and control distinct reflexes, we discovered that point-to-point and parallel visual circuits emerge independently. Disruption of any one set of connections did not alter the adjacent parallel pathway at the level of axon-target matching, downstream circuit wiring, or function. Specifically, we found that $Tph2^{Cre}$-mediated ablation of Tbr2 RGCs leads to a massive reduction of luminance-sensing input to the OPN and mdPPN. Nevertheless, the newly available territory in these targets was still avoided by other RGC types, such as slow- and On-Off DSGCs. Moreover, circuits downstream of the deafferented targets maintained functionality in response to chemogenetic stimulation, highlighting the extent to which each point-to-point connection in this system wires up independently.

A minimum of RGCs is sufficient to drive PLR behavior

Some ipRGCs escape our genetic ablation and even though they provide minimal input to the OPN in cKOs, remarkably, they can drive the PLR circuit when it is stimulated by high intensity, short-wavelength light. Indeed, the remaining few retinal afferents drove maximal constriction in a manner similar to wildtype animals. This indicates that the degree of reflex-generating excitation at retina-to-OPN synapses is likely to be extremely reliable. The implication therefore is that entry of any abnormal RGC afferents to this target would be highly disruptive to the function of the circuit because the receptive field properties of those mis-projecting cells (e.g., DSGCs) would then drive the PLR under abnormal conditions. Protecting reflex circuits from abnormal afferent entry and function therefore may be a general property of mammalian CNS circuits set up by the availability of guidance cues.

Cellular and molecular constraints on parallel pathway wiring

Previous work demonstrated that Cre-dependent removal of Tbr2 leads to RGC death, with ipRGCs particularly susceptible and to reduced retinal innervation of several targets, including OPN and mdPPN (Mao et al., 2008; 2014; Sweeney et al., 2014). Here we used the $Tph2^{Cre}$ line to delete Tbr2 and because of its projection pattern in pretectum as well as its overlap with Tbr2 and luminance-sensing RGCs, the Tbr2 mutation eliminated virtually all retinal input to the OPN and mdPPN without affecting retinal innervation of the neighboring NOT. Our examination of projections from genetically labeled RGC types following the loss of Tbr2 provides insight into subsequent changes to specific retinal populations and their central projections.

How might the developmental timing of RGC axon growth impact axon-target stringency in the visual brainstem? Cdh3-RGC axons are some of the first retinal projections to enter the brain and thus represent '*pioneers*'; they grow through a relatively axon-free environment compared to later-arriving RGC axons, allowing them ample opportunity to innervate retinorecipient targets as well as transiently enter inappropriate nuclei along the way, which they do (Osterhout et al., 2014). In theory, because luminance-sensing RGCs enter and establish themselves in pretectal targets as well as transiently mis-wire to other RGC targets we expected that their early, large-scale removal would allow other RGC axons to take over vacated OPN and mdPPN ('*axon competition*'; Figure 1D). This was not the case, however; a normal innervation pattern of slow- and On-Off DSGCs persisted with reduced luminance-sensing retinal input to pretectum following genetic ablation. So rather than competitive interactions, axon-target matching in developing parallel pathways is likely governed by molecular matching mechanisms that do not tolerate cross-wiring. Molecular regulation of navigating axons prevents wiring errors that could potentially compromise normal function. This is distinct from eye-specific and retinotopic mapping which do involve competitive interactions (Huberman et al., 2008) and is similar to '*stringent specificity*' described for cell-cell target specific matching in the spinal system (Betley et al., 2009; Figure 1E).

Studies from several labs have begun to reveal some of the targeting molecules and receptors involved in axon-target matching in the mouse visual system (Osterhout et al., 2011; 2015; Su et al., 2011; 2013; Sun et al., 2015). Disruption of these molecular-mediated attractive forces results in diminished axonal termination within their proper central targets and misrouted axons, suggesting that RGCs fail to recognize and innervate their proper targets. For example, the adhesion molecule, cadherin-6 (Cdh6) is expressed both by Cdh3-RGCs as well as cells in their central targets such as OPN and in Cdh6 mutant mice Cdh3-RGC axons display targeting deficits (Osterhout et al., 2011). Perhaps slow-DSGCs are not able to enter the vacant OPN and mdPPN in Tbr2 cKOs because they lack an attractive or adhesive cue, such as Cdh6. A non-mutually exclusive explanation is that, regardless of OPN availability, the expression of adhesive cues such as contactin-4 (Osterhout et al., 2015) and attractive guidance cues like members of the semaphorin-plexin family of axon guidance molecules (Sun et al., 2015) allows slow-DSGCs to select the NOT and other targets appropriate for their function because those targets are more molecularly attractive for that RGC type. Even though newly available territory in OPN is accessible following the loss of luminance-sensing RGCs, the continued presence of the normal pretectal target for slow-DSGCs may prevent miswiring of these RGC axons. Earlier studies examining miswiring of connections across different sensory modalities demonstrated that cross-wiring is unable to occur by merely opening up space in a nearby target. Only when targets are vacated and the normal target is ablated do axons go into the incorrect target (Roe et al., 1990; Sur et al., 1990; von Melchner et al., 2000).

Light-intensity-dependent influences on PLR behavior in ipRGC deficient mice

We examined the functional output of retinal-OPN connections in cKOs and found that the effect of losing luminance-sensing input on PLR was dependent on light intensity. Under lower light conditions, PLR was significantly perturbed following genetic ablation of luminance-sensing RGCs. When we used very high intensity blue light or sustained

chemogenetic activation of RGCs or OPN neurons, PLR was unaffected in cKOs. This is comparable to what was previously seen for *Tbr2*$^{flox/flox}$:*Opn4*$^{Cre/+}$:*Z/EG* mice (Mao et al., 2014). These mice lose 90% of ipRGCs and exhibit only a mild deficit in pupil constriction compared to wildtype mice when using high irradiance levels.

Finally, how does the behavioral output of the PLR pathway function relatively normally with negligible retinal input? The answer to this question has relevance to understanding how poly-synaptic circuits wire up and maintain plasticity in the mammalian brain. One possibility is that high intensity light can maximally drive the remaining luminance-sensing RGCs to provide normal functional output. Consistent with this, an earlier study determined that only about 17% of ipRGCs are necessary to drive full pupil constriction (Güler et al., 2008). Other contributing factors might possibly arise from changes within the OPN itself, either OPN neurons or nonretinal afferents from other areas of the brain, and/or alterations in the downstream cells and connections within the PLR pathway. Our experiments retrogradely labeling OPN cells from EW revealed that those projection neurons are present and appear normal in connectivity in cKOs. Studies in rat (Jeffery, 1984) and ferret (Crowley and Katz, 1999; 2000) demonstrated that some features of geniculocortical projections are preserved following early eye removal. Taken together with our results this suggests that early loss of retinal input does not lead to postsynaptic neuronal death in subcortical targets. However, the significant reduction of PV expression in the OPN reveals that targets do alter their internal circuitry and/or molecular expression in response to deafferentation. The consequence of diminished PV on OPN functional output requires further investigation and the cell type specific efferent connections of OPN are yet to be clearly defined.

Conclusions and implications for regeneration

Our study unveils a remarkable refractoriness of visual parallel pathways and their downstream circuits to selective loss of one set of sensory afferents during development. This resilience makes sense in light of the adaptive nature of sensory-driven adaptive reflexes such as the PLR and optokinetic reflex (OKR). Developmental constraints such as those described here are critical for models of regeneration, which is essentially an attempt to recapitulate developmental wiring, albeit to varying degrees depending on the lesion size and location (Laha et al., 2017). The findings presented here are consistent with the re-establishment of retino-OPN and retino-AOS connectivity observed in RGCs stimulated to regenerate by combined mTOR enhancement and neural activity (Lim et al., 2016). In that study, regenerating RGCs were able to pathfind back to their targets and restore behaviors. Thus, target specificity of retinal axons controlling reflexive behaviors appears to be firmly hard-wired and resistant to perturbations that might compromise the functional output of their pathways.

EXPERIMENTAL PROCEDURES

Animals

Mice of either sex were used and ranged in age from E13.5 to 2-months old. Cdh3-GFP (Osterhout et al., 2011), Opn4-GFP (Lim et al., 2016), Hoxd10-GFP (Dhande et al., 2013), DRD4-GFP (Rivlin-Etzion et al., 2011), TRHR-GFP (Huberman et al., 2009; Rivlin-Etzion

et al., 2011), CB2-GFP (Huberman et al., 2008b), and Tph2^{Cre} (stock no. 036634-UCD) mouse lines were obtained from MMRRC. The floxed Tbr2 line (stock no. 017293) was acquired from Jackson Laboratory. Animals were housed on a 12h light/dark cycle, behavior was done at consistent hours during the light cycle. All experimental procedures were in accordance with NIH guidelines and approved by the Institutional Animal Care and Use Committees at the University of California, San Diego and Stanford University School of Medicine.

Intravitreal injections of tracers and viruses

1-2μL of AAV2-hSyn-DIO-hM3D(G_q)-mCherry or AAV2-hSyn-hM3D(G1)-IRES-mCitrine (UNC Gene Therapy Vector Core) or the CTb conjugated to Alexa Fluor 488, 594 or 647 (Invitrogen) were injected into the vitreal chamber of the eye using a Hamilton syringe as described previously (Huberman et al., 2008b). CTb-injected animals were given a 1–2d survival period to allow tracer to travel down and label all RGC axons. AAV-injected animals were given 3–4w survival period to allow for virus experssion.

Stereotaxic brain injections of viruses

Stereotaxic injections of virus (~100nl) were made with a small glass pipette attached to a Nanoject II (Drummond). ΔG-RABV-mCherry (GT3 Core Facility of the Salk Institute) was injected into EW to label presynaptic cells within OPN (midline, 3.8mm posterior to Bregma, 3.1 mm from pial surface). To retrogradely label RGCs from OPN, ΔG-RABV-mCherry was injected 0.6mm lateral to midline, 2.5mm posterior to Bregma and 2.25mm from the pial surface. A 4–5d survival period was given to allow rabies to infect and express mCherry in presynaptic cells. To express hM3D in OPN cells, AAV8-hSyn-hM3D(G_q)-mCherry (UNC Gene Therapy Vector Core), was injected at the coordinates stated above and mice had a 3–4w survival time.

Immunohistochemistry

Mice were transcardially perfused, brains were harvested and postfixed in 4% paraformaldehyde (PFA)(24h at 4°C), then sectioned coronally at 45μm following cryoprotection with 30% sucrose. Eyes were removed, postfixed in 4% PFA (4h,at 4°C), then the retina was extracted and relieving cuts were made to allow it to lay flat.

To isolate embryos, impregnated animals were euthanized and the uterus was dissected out. Embryos were removed, separated from the placenta and yolk sac, then postfixed in 4% PFA (24h at 4°C). Following cryoprotection, embryo heads were embedded in Tissue-Tek O.C.T. compound (Sakura), 25μm cross sections were made using a cryostat.

Tissue was incubated overnight at 4°C in primary antibodies and incubated for 2h at room temperature with appropriate secondary antibodies. Primary antibodies: chicken anti-GFP (1:1,000; Aves Labs, GFP-1020), goat anti-GFP (1:2,000, Abcam, ab6673), rabbit anti-GFP (1:1,000; Invitrogen, A6455), rabbit anti-melanopsin (1:1,000; Advanced Targeting Systems, AB-N39), mouse anti-PV (1:1,000; Sigma, P3088), guinea pig anti-RBPMS (1:2,000; PhosphoSolutions, 1832-RBPMS), rabbit anti-RBPMS (1:2,000; PhosphoSolutions, 1830-RBPMS), chicken anti-Tbr2 (1:1,000; Millipore, AB15894), rabbit anti-Tbr2 (1:1,000;

Abcam, ab23345). Species-specific secondary antibodies conjugated to Alexa Fluor 488, 594 or 647 (1:1000, Invitrogen and Jackson Laboratory) were used. For Nissl staining, sections were incubated in NeuroTrace 530/615 (1:100 in PBS; ThermoFisher Scientific, N21482) for 20 min.

Quantification of percentage of target area occupied by GFP-expressing axons

Area fraction measurements were quantified in ImageJ as described previously (Osterhout et al., 2014). Background was measured and subtracted. The *area fraction* tool was used to find the % of target occupied by GFP^+ axons. Measurements were taken from 2–5 tissue sections depending on target size and age.

Cell number quantification

Cell counts were taken from 3–5 sections containing OPN. All PV^+ cells in OPN within the plane of focus were counted. An automated cell counter in ImageJ determined the total cell number (Nissl bodies) within a 200μm × 200μm area of OPN.

Pupillometry

Mice were dark-adapted in their home cage for 2h prior and experiments were performed under infrared illumination. Unanesthetized mice, previously habituated to handling to minimize stress, were gently restrained by hand for the duration of recordings. For light-induced PLR, a single blue LED (470nm; Thorlabs, M470L3) was placed approximately 4cm from one eye. An infrared camcorder (Panasonic, HC-W850) placed on the opposite side of the head recorded the pupil before, during and after light stimulus. For chemogenetic-induced PLR, mice were in the dark for the entirety of the experiment and the pupil was recorded before and following injection of clozapine-*N*-oxide (CNO; I.P., 1mg/kg; Tocris Bioscience; dissolved at 1mg/ml in DMSO (0.5%)/saline). For light- and chemogenetic-induced PLR, the consensual pupil response of the eye contralateral to the stimulated eye was recorded.

PLR data analysis

Individual frames were extracted from videos to quantify pupil size. For light-induced PLR, frames were extracted every 5s from t = −5s to t = 50s. Pupil diameter was calculated for each frame and normalized to the diameter of the eye in the same frame in ImageJ. Pupil area was calculated for each time point relative to the initial dark adapted pupil size (t = −5s). For chemogenetic-induced PLR, frames were extracted before CNO (pre-) and 1h following CNO injection (post-). The post-CNO pupil area was calculated relative to pre-CNO pupil size.

Statistical analysis

To determine statistical significance, we used Student's *t*-test for comparing 2 groups of mice (WT versus cKO). Statistical tests were performed with Prism v6 software (GraphPad). All data in graphs represent mean ± SEM. The level of significance was set at $p < 0.05$.

Supplementary Material

Refer to Web version on PubMed Central for supplementary material.

Acknowledgments

We thank Victoria Cheung and Ann Phan for their help with imaging and data analysis. We are grateful to the members of the Huberman lab for their helpful comments on the manuscript. This work was supported by grants from the National Eye Institute of the National Institutes of Health, NEI-NIH F32-EY025530 (T.A.S.), R01-EY022157 (A.D.H.), and R01-EY026100 (A.D.H.).

References

Abraira VE, Ginty DD. 2013; The sensory neurons of touch. Neuron. 79:618–639. [PubMed: 23972592]

Anderson DJ. 2016; Circuit modules linking internal states and social behaviour in flies and mice. Nat Rev Neurosci. 17:692–704. [PubMed: 27752072]

Arber S. 2012; Motor circuits in action: specification, connectivity, and function. Neuron. 74:975–989. [PubMed: 22726829]

Betley JN, Wright CV, Kawaguchi Y, Erdélyi F, Szabó G, Jessell TM, Kaltschmidt JA. 2009; Stringent specificity in the construction of a GABAergic presynaptic inhibitory circuit. Cell. 139:161–174. [PubMed: 19804761]

Bonanomi D, Pfaff SL. 2010; Motor axon pathfinding. Cold Spring Harb Perspect Biol. 2:a001735. [PubMed: 20300210]

Campbell FW, Gregory AH. 1960; Effect of size of pupil on visual acuity. Nature. 187:1121–1123.

Cang J, Feldheim DA. 2013; Developmental mechanisms of topographic map formation and alignment. Annu Rev Neurosci. 36:51–77. [PubMed: 23642132]

Chen SK, Badea TC, Hattar S. 2011; Photoentrainment and pupillary light reflex are mediated by distinct populations of ipRGCs. Nature. 476:92–95. [PubMed: 21765429]

Clark DA, Freifeld L, Clandinin TR. 2013; Mapping and cracking sensorimotor circuits in genetic model organisms. Neuron. 78:583–595. [PubMed: 23719159]

Crowley JC, Katz LC. 1999; Development of ocular dominance columns in the absence of retinal input. Nat Neurosci. 2:1125–1130. [PubMed: 10570491]

Crowley JC, Katz LC. 2000; Early development of ocular dominance columns. Science. 290:1321–1324. [PubMed: 11082053]

Davidson S, Giesler GJ. 2010; The multiple pathways for itch and their interactions with pain. Trends Neurosci. 33:550–558. [PubMed: 21056479]

De Franceschi G, Vivattanasarn T, Saleem AB, Solomon SG. 2016; Vision guides selection of freeze or flight defense strategies in mice. Curr Biol. 26:2150–2154. [PubMed: 27498569]

Dhande OS, Estevez ME, Quattrochi LE, El-Danaf RN, Nguyen PL, Berson DM, Huberman AD. 2013; Genetic dissection of retinal inputs to brainstem nuclei controlling image stabilization. J Neurosci. 33:17797–17813. [PubMed: 24198370]

Dhande OS, Huberman AD. 2014; Retinal ganglion cell maps in the brain: implications for visual processing. Curr Opin Neurobiol. 24:133–142. [PubMed: 24492089]

Dhande OS, Stafford BK, Lim JHA, Huberman AD. 2015; Contributions of retinal ganglion cells to subcortical visual processing and behaviors. Annu Rev Vis Sci. 1:291–328. [PubMed: 28532372]

Do MT, Yau KW. 2010; Intrinsically photosensitive retinal ganglion cells. Physiol Rev. 90:1547–1581. [PubMed: 20959623]

Dodd J, Jessell TM. 1988; Axon guidance and the patterning of neuronal projections in vertebrates. Science. 242:692–699. [PubMed: 3055291]

Dräger UC. 1985; Birth dates of retinal ganglion cells giving rise to the crossed and uncrossed optic projections in the mouse. Proc R Soc Lond B Biol Sci. 224:57–77. [PubMed: 2581263]

Erskine L, Herrera E. 2014; Connecting the retina to the brain. ASN Neuro. 6

Fenno L, Yizhar O, Deisseroth K. 2011; The development and application of optogenetics. Annu Rev Neurosci. 34:389–412. [PubMed: 21692661]

Fields HL, Heinricher MM. 1989; Brainstem modulation of nociceptor-driven withdrawal reflexes. Ann N Y Acad Sci. 563:34–44. [PubMed: 2672950]

Gamlin PDR. 2006; The pretectum: connections and oculomotor-related roles. Prog Brain Res. 151:379–405. [PubMed: 16221595]

Gong S, Doughty M, Harbaugh CR, Cummins A, Hatten ME, Heintz N, Gerfen CR. 2007; Targeting CRE recombinase to specific neuron populations with Bacterial Artificial Chromosome constructs. J Neurosci. 27:9817–9823. [PubMed: 17855595]

Güler AD, Ecker JL, Lall GS, Haq S, Altimus CM, Liao HW, Barnard AR, Cahill H, Badea TC, Zhao H, et al. 2008; Melanopsin cells are the principal conduits for rod-cone input to non-image-forming vision. Nature. 453:102–105. [PubMed: 18432195]

Han L, Dong X. 2014; Itch mechanisms and circuits. Annu Rev Biophys. 43:331–355. [PubMed: 24819620]

Hashikawa K, Hashikawa Y, Falkner A, Lin D. 2016; The neural circuits of mating and fighting in male mice. Curr Opin Neurobiol. 38:27–37. [PubMed: 26849838]

Hatori M, Le H, Vollmers C, Keding SR, Tanaka N, Buch T, Waisman A, Schmedt C, Jegla T, Panda S. 2008; Inducible ablation of melanopsin-expressing retinal ganglion cells reveals their central role in non-image forming visual responses. PLoS One. 3:e2451. [PubMed: 18545654]

Huberman AD, Feller MB, Chapman B. 2008a; Mechanisms Underlying Development of Visual Maps and Receptive Fields. Annu Rev Neurosci. 31:479–509. [PubMed: 18558864]

Huberman AD, Manu M, Koch SM, Susman MW, Lutz AB, Ullian EM, Baccus SA, Barres BA. 2008b; Architecture and activity-mediated refinement of axonal projections from a mosaic of genetically identified retinal ganglion cells. Neuron. 59:425–438. [PubMed: 18701068]

Huberman AD, Wei W, Elstrott J, Stafford BK, Feller MB, Barres BA. 2009; Genetic identification of an On-Off direction-selective retinal ganglion cell subtype reveals a layer-specific subcortical map of posterior motion. Neuron. 62:327–334. [PubMed: 19447089]

Hufnagel RB, Le TT, Riesenberg AL, Brown NL. 2010; Neurog2 controls the leading edge of neurogenesis in the mammalian retina. Dev Biol. 340:490–503. [PubMed: 20144606]

Jeffery G. 1984; Transneuronal effects of early eye removal on geniculo-cortical projection cells. Brain Res. 315:257–263. [PubMed: 6722589]

Kolodkin AL, Tessier-Lavigne M. 2011; Mechanisms and molecules of neuronal wiring: a primer. Cold Spring Harb Perspect Biol. 3

Kobayakawa K, Kobayakawa R, Matsumoto H, Oka Y, Imai T, Ikawa M, Okabe M, Ikeda T, Itohara S, Kikusui T, et al. 2007; Innate versus learned odour processing in the mouse olfactory bulb. Nature. 450:503–508. [PubMed: 17989651]

Laha B, Stafford BK, Huberman AD. 2017; Regenerating optic pathways from the eye to the brain. Science. 356:1031–1034. [PubMed: 28596336]

Lim JH, Stafford BK, Nguyen PL, Lien BV, Wang C, Zukor K, He Z, Huberman AD. 2016; Neural activity promotes long-distance, target-specific regeneration of adult retinal axons. Nat Neurosci. 19:1073–1084. [PubMed: 27399843]

Lucas RJ, Hattar S, Takao M, Berson DM, Foster RG, Yau KW. 2003; Diminished pupillary light reflex at high irradiances in melanopsin-knockout mice. Science. 299:245–247. [PubMed: 12522249]

Luo L, Flanagan JG. 2007; Development of continuous and discrete neural maps. Neuron. 56:284–300. [PubMed: 17964246]

Madisen L, Mao T, Koch H, Zhuo JM, Berenyi A, Fujisawa S, Hsu YW, Garcia AJ 3rd, Gu X, Zanella S, et al. 2012; A toolbox of Cre-dependent optogenetic transgenic mice for light-induced activation and silencing. Nat Neurosci. 15:793–802. [PubMed: 22446880]

Mao CA, Kiyama T, Pan P, Furuta Y, Hadjantonakis AK, Klein WH. 2008; Eomesodermin, a target gene of Pou4f2, is required for retinal ganglion cell and optic nerve development in the mouse. Development. 135:271–280. [PubMed: 18077589]

Mao CA, Li H, Zhang Z, Kiyama T, Panda S, Hattar S, Ribelayga CP, Mills SL, Wang SW. 2014; T-box transcription regulator Tbr2 is essential for the formation and maintenance of Opn4/

melanopsin-expressing intrinsically photosensitive retinal ganglion cells. J Neurosci. 34:13083–13095. [PubMed: 25253855]

Morin LP, Studholme KM. 2014; Retinofugal projections in the mouse. J Comp Neurol. 522:3733–3753. [PubMed: 24889098]

O'Leary DD, Yates PA, McLaughlin T. 1999; Molecular development of sensory maps: representing sights and smells in the brain. Cell. 96:255–269. [PubMed: 9988220]

Osterhout JA, Josten N, Yamada J, Pan F, Wu SW, Nguyen PL, Panagiotakos G, Inoue YU, Egusa SF, Volgyi B, et al. 2011; Cadherin-6 mediates axon-target matching in a non-image-forming visual circuit. Neuron. 71:632–639. [PubMed: 21867880]

Osterhout JA, El-Danaf RN, Nguyen PL, Huberman AD. 2014; Birthdate and outgrowth timing predict cellular mechanisms of axon target matching in the developing visual pathway. Cell Rep. 8:1006–1017. [PubMed: 25088424]

Osterhout JA, Stafford BK, Nguyen PL, Yoshihara Y, Huberman AD. 2015; Contactin-4 mediates axon-target specificity and functional development of the accessory optic system. Neuron. 86:985–999. [PubMed: 25959733]

Polleux F, Snider W. 2010; Initiating and Growing an Axon. Cold Spring Harb Perspect Biol. 2:a001925. [PubMed: 20452947]

Prichard JR, Stoffel RT, Quimby DL, Obermeyer WH, Benca RM, Behan M. 2002; Fos immunoreactivity in rat subcortical visual shell in response to illuminance changes. Neuroscience. 114:781–793. [PubMed: 12220578]

Raper J, Mason C. 2010; Cellular strategies of axonal pathfinding. Cold Spring Harb Perspect Biol. 2:a001933. [PubMed: 20591992]

Riccomagno MM, Kolodkin AL. 2015; Sculpting neural circuits by axon and dendrite pruning. Annu Rev Cell Dev Biol. 31:779–805. [PubMed: 26436703]

Rivlin-Etzion M, Zhou K, Wei W, Elstrott J, Nguyen PL, Barres BA, Huberman AD, Feller MB. 2011; Transgenic mice reveal unexpected diversity of on-off direction-selective retinal ganglion cell subtypes and brain structures involved in motion processing. J Neurosci. 31:8760–8769. [PubMed: 21677160]

Rodriguez AR, de Sevilla Müller LP, Brecha NC. 2014; The RNA binding protein RBPMS is a selective marker of ganglion cells in the mammalian retina. J Comp Neurol. 522:1411–1443. [PubMed: 24318667]

Roe AW, Pallas SL, Hahm JO, Sur M. 1990; A map of visual space induced in primary auditory cortex. Science. 250:818–820. [PubMed: 2237432]

Rossignol S, Dubuc R, Gossard JP. 2006; Dynamic sensorimotor interactions in locomotion. Physiol Rev. 86:89–154. [PubMed: 16371596]

Sanes JR, Lichtman JW. 1999; Development of the vertebrate neuromuscular junction. Annu Rev Neurosci. 22:389–442. [PubMed: 10202544]

Sanes JR, Yamagata M. 2009; Many paths to synaptic specificity. Annu Rev Cell Dev Biol. 25:161–195. [PubMed: 19575668]

Schmidt TM, Do MT, Dacey D, Lucas R, Hattar S, Matynia A. 2011; Melanopsin-positive intrinsically photosensitive retinal ganglion cells: from form to function. J Neurosci. 31:16094–16101. [PubMed: 22072661]

Schneider VA, Granato M. 2003; Motor axon migration: a long way to go. Dev Biol. 263:1–11. [PubMed: 14568542]

Seabrook TA, Burbridge TJ, Crair MC, Huberman AD. 2017; Architecture, Function, and Assembly of the Mouse Visual System. Annu Rev Neurosci. 40:499–538. [PubMed: 28772103]

Shatz CJ, Sretavan DW. 1986; Interactions between retinal ganglion cells during the development of the mammalian visual system. Annu Rev Neurosci. 9:171–207. [PubMed: 2423004]

Simpson JI. 1984; The accessory optic system. Annu Rev Neurosci. 7:13–41. [PubMed: 6370078]

Sretavan DW. 1990; Specific routing of retinal ganglion cell axons at the mammalian optic chiasm during embryonic development. J Neurosci. 10:1995–2007. [PubMed: 2162389]

Stowers L, Cameron P, Keller JA. 2013; Ominous odors: olfactory control of instinctive fear and aggression in mice. Curr Opin Neurobiol. 23:339–345. [PubMed: 23415829]

Stowers L, Liberles SD. 2016; State-dependent responses to sex pheromones in mouse. Curr Opin Neurobiol. 38:74–79. [PubMed: 27093585]

Su J, Haner CV, Imbery TE, Brooks JM, Morhardt DR, Gorse K, Guido W, Fox MA. 2011; Reelin is required for class-specific retinogeniculate targeting. J Neurosci. 31:575–586. [PubMed: 21228166]

Su J, Klemm MA, Josephson AM, Fox MA. 2013; Contributions of VLDLR and LRP8 in the establishment of retinogeniculate projections. Neural Dev. 8:11. [PubMed: 23758727]

Sun LO, Brady CM, Cahill H, Al-Khindi T, Sakuta H, Dhande OS, Noda M, Huberman AD, Nathans J, Kolodkin AL. 2015; Functional assembly of accessory optic system circuitry critical for compensatory eye movements. Neuron. 86:971–984. [PubMed: 25959730]

Sur M, Pallas SL, Roe AW. 1990; Cross-modal plasticity in cortical development: differentiation and specification of sensory neocortex. Trends Neurosci. 13:227–233. [PubMed: 1694329]

Sweeney NT, Tierney H, Feldheim DA. 2014; Tbr2 is required to generate a neural circuit mediating the pupillary light reflex. J Neurosci. 34:5447–5453. [PubMed: 24741035]

Urban DJ, Roth BL. 2015; DREADDs (designer receptors exclusively activated by designer drugs): chemogenetic tools with therapeutic utility. Annu Rev Pharmacol Toxicol. 55:399–417. [PubMed: 25292433]

von Melchner L, Pallas SL, Sur M. 2000; Visual behaviour mediated by retinal projections directed to the auditory pathway. Nature. 404:871–876. [PubMed: 10786793]

Whissell PD, Tohyama S, Martin LJ. 2016; The Use of DREADDs to Deconstruct Behavior. Front Genet. 7:70. [PubMed: 27242888]

Williams SE, Mason CA, Herrera E. 2004; The optic chiasm as a midline choice point. Curr Opin Neurobiol. 14:51–60. [PubMed: 15018938]

Yang T, Shah NM. 2016; Molecular and neural control of sexually dimorphic social behaviors. Curr Opin Neurobiol. 38:89–95. [PubMed: 27162162]

Yilmaz M, Meister M. 2013; Rapid innate defensive responses of mice to looming visual stimuli. Curr Biol. 23:2011–2015. [PubMed: 24120636]

Yonehara K, Ishikane H, Sakuta H, Shintani T, Nakamura-Yonehara K, Kamiji NL, Usui S, Noda M. 2009; Identification of retinal ganglion cells and their projections involved in central transmission of information about upward and downward image motion. PLoS One. 4:e4320. [PubMed: 19177171]

Zhang C, Kolodkin AL, Wong RO, James RE. 2017; Establishing Wiring Specificity in Visual System Circuits: From the Retina to the Brain. Annu Rev Neurosci. 40:395–424. [PubMed: 28460185]

Zhao X, Liu M, Cang J. 2014; Visual cortex modulates the magnitude but not the selectivity of looming-evoked responses in the superior colliculus of awake mice. Neuron. 84:202–213. [PubMed: 25220812]

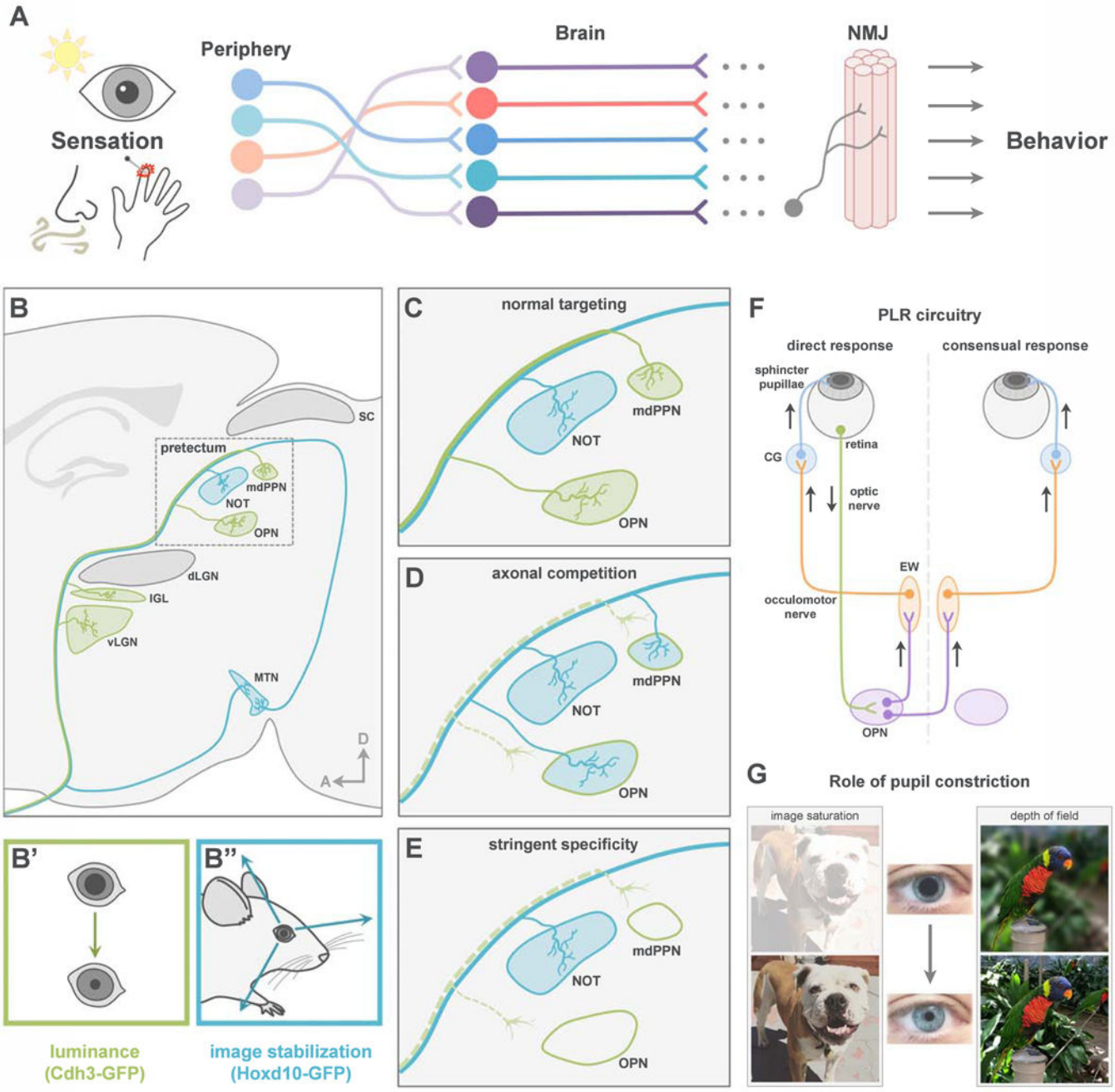

Figure 1. Retinal connections to pretectum and circuitry controlling pupillary light reflex

(A) Sensations drive adaptive behaviors via pathways from peripheral sensory neurons to the NMJ. (B) Projection pattern of functionally distinct RGC subtypes. dLGN, dorsal lateral geniculate nucleus; IGL, intergeniculate nucleus; vLGN, ventral lateral geniculate nucleus; mdPPN, medial division of the posterior pretectal nucleus; MTN, medial terminal nucleus; NOT, nucleus of the optic tract; OPN, olivary pretectal nucleus; SC, superior colliculus. (C) Normal RGC targeting of pretectum. (D–E) Potential outcomes of losing luminance-sensing RGC input. (F) Schematic of PLR circuit. CG, ciliary ganglion; EW, Edinger-Westphal nucleus; OPN, olivary pretectal nucleus. (G) Role of pupil constriction.

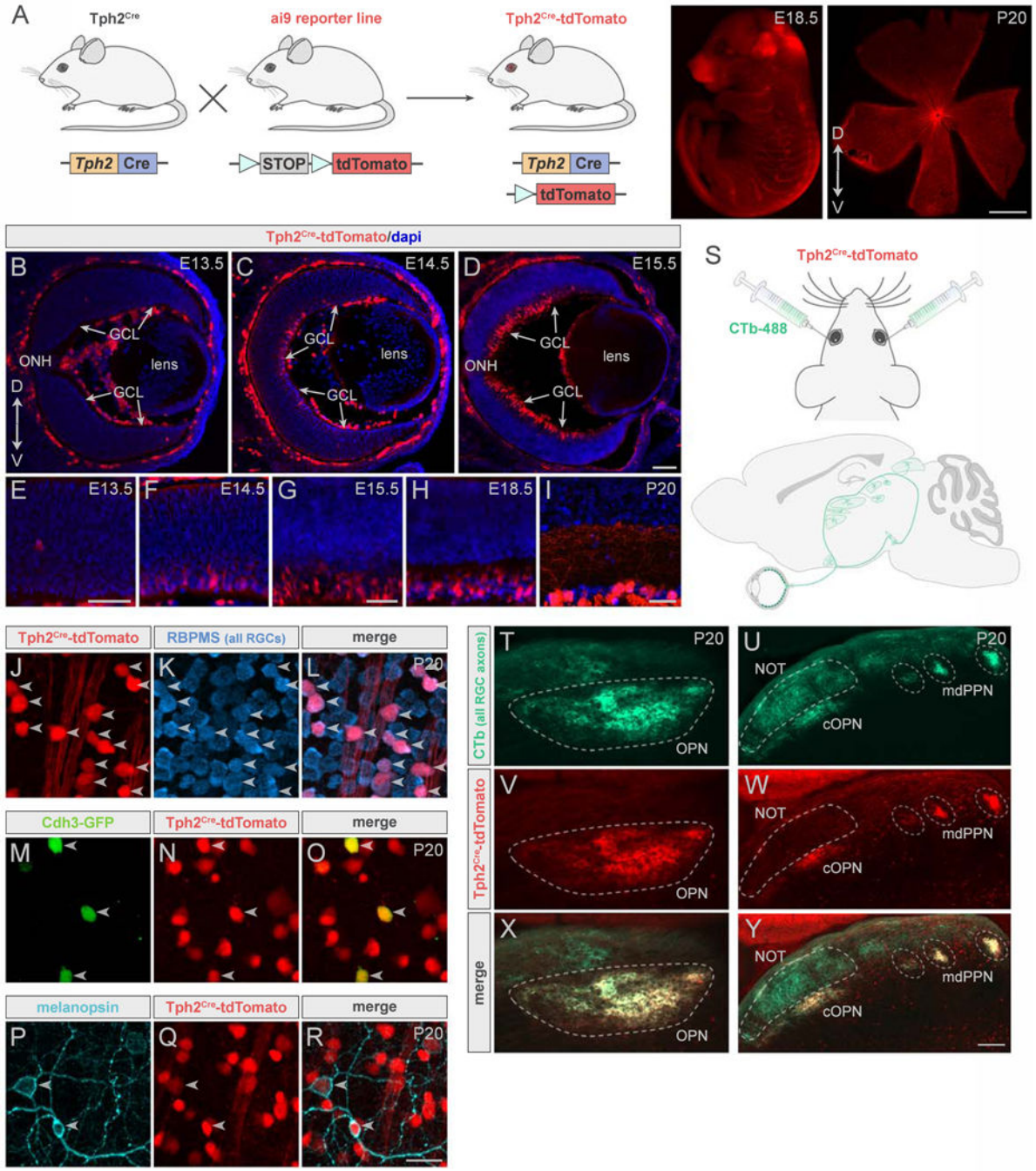

Figure 2. Tph2^{Cre} allows for manipulation of luminance-sensing RGCs

(A) Cre^{+} mice crossed to a reporter line to visualize Tph2^{Cre}. Right panels, Tph2^{Cre} - tdTomato (red) in embryo and whole-mount retina. Scale bar, 800μm. (B–I) Developmental retinal expression of Tph2^{Cre}. (B–D) Transverse cryosections of eye at different embryonic ages. GCL, ganglion cell layer; ONH, optic nerve head. Scale bar, 50μm (B), 100μm (C and D). (E–I), High-magnification images of cryosections. Scale bars, 50μm. (J–R) Whole-mount retinas from Tph2^{Cre} mice. (J–L) Cre cells (red) stain for RGC marker, RBPMS (blue). (M–O) 90% of Cdh3-GFP RGCs (green) express Tph2^{Cre} (red). (P–R) 84% of

melanopsin^{+} RGCs (cyan) express Tph2^{Cre} (red). Arrowheads indicate colabeling. Scale bar, 25μm. (S) Eyes of Tph2^{Cre}-tdTomato mice were injected with CTb-488 (green). (T–Y) All RGC (CTb, green) and Tph2^{Cre} RGC (red) axons in pretectum. Scale bar, 200μm (T, V, X); 100μm (U, W, Y). mdPPN, medial division of the posterior pretectal nucleus; NOT, nucleus of the optic tract; OPN, olivary pretectal nucleus; cOPN, caudal OPN.

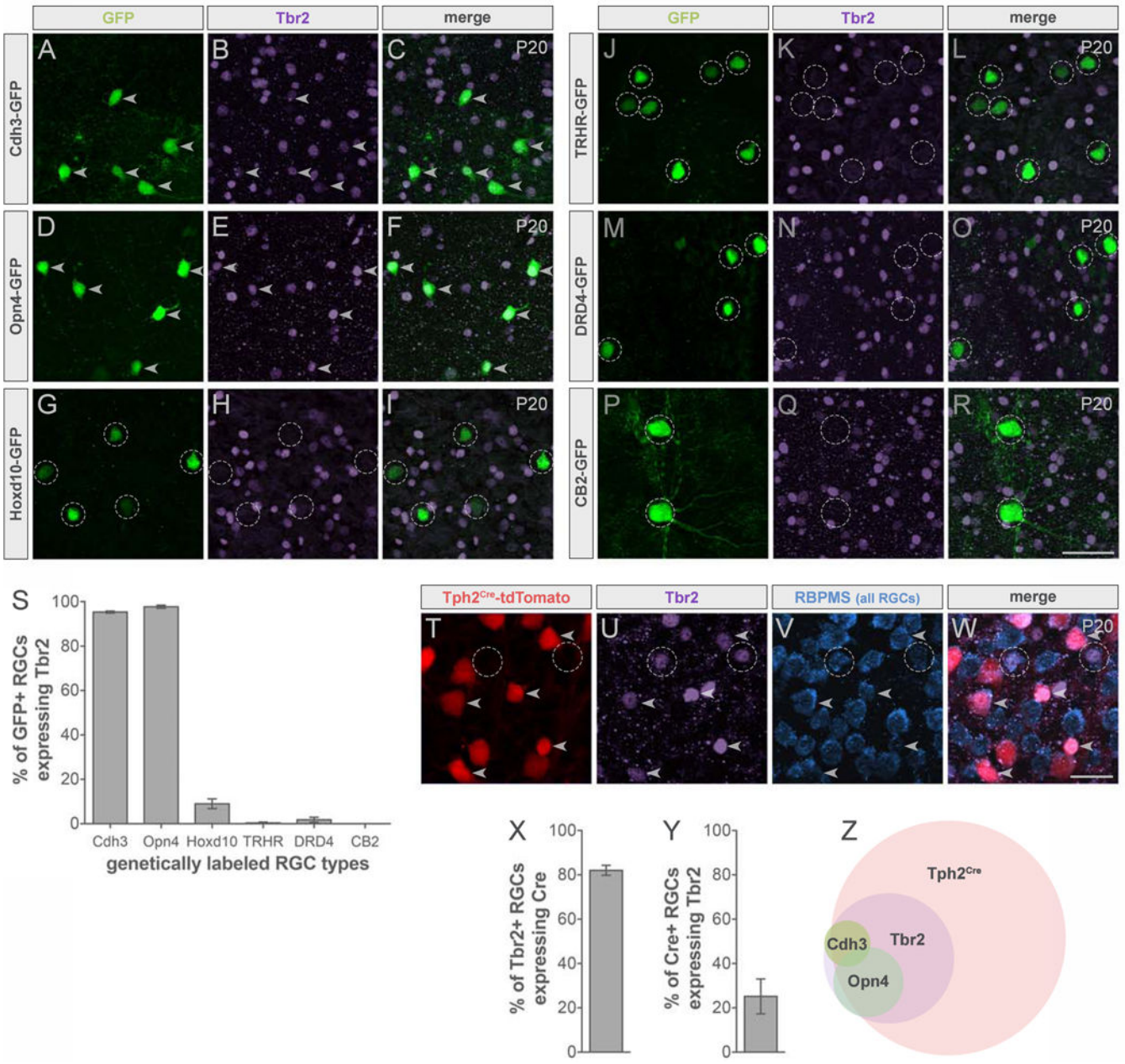

Figure 3. Tbr2 is expressed by a subset of RGCs

(A–R) Whole-mount retinas from transgenic mice expressing GFP in different RGC subtypes (green) immunostained for Tbr2 (purple). Luminance-sensing: Cdh3-GFP (A–C), Opn4-GFP (D–F); image-stabilizing: Hoxd10-GFP (G–I); posterior-tuned On-Off DSGCs: TRHR-GFP (J–L), DRD4-GFP (M–O); transient-OFF alpha RGCs: CB2-GFP (P–R). Arrowheads indicate colabeling and dashed circles indicate GFP only. Scale bar, 50μm. (S) Quantification of % of GFP^+ RGCs expressing Tbr2. Data are represented as mean ± SEM (n = 2–3 mice). (T–W) Retinas from $Tph2^{Cre}$-tdTomato mice immunostained for Tbr2 and RBPMS. Arrowheads indicate $Tph2^{Cre}$ expression in $Tbr2^+$ RGCs ($RBPMS^+$) and dashed circles indicate $Tbr2^+$ RGCs only. Scale bar, 25μm. (X) Quantification of % of $Tbr2^+$ RGCs

expressing $Tph2^{Cre}$. (Y) % of $Tph2^{Cre}$ RGCs expressing Tbr2. Data are represented as mean ± SEM (n = 3 mice). (Z) Summary Venn diagram. See also Figures S1 and S2.

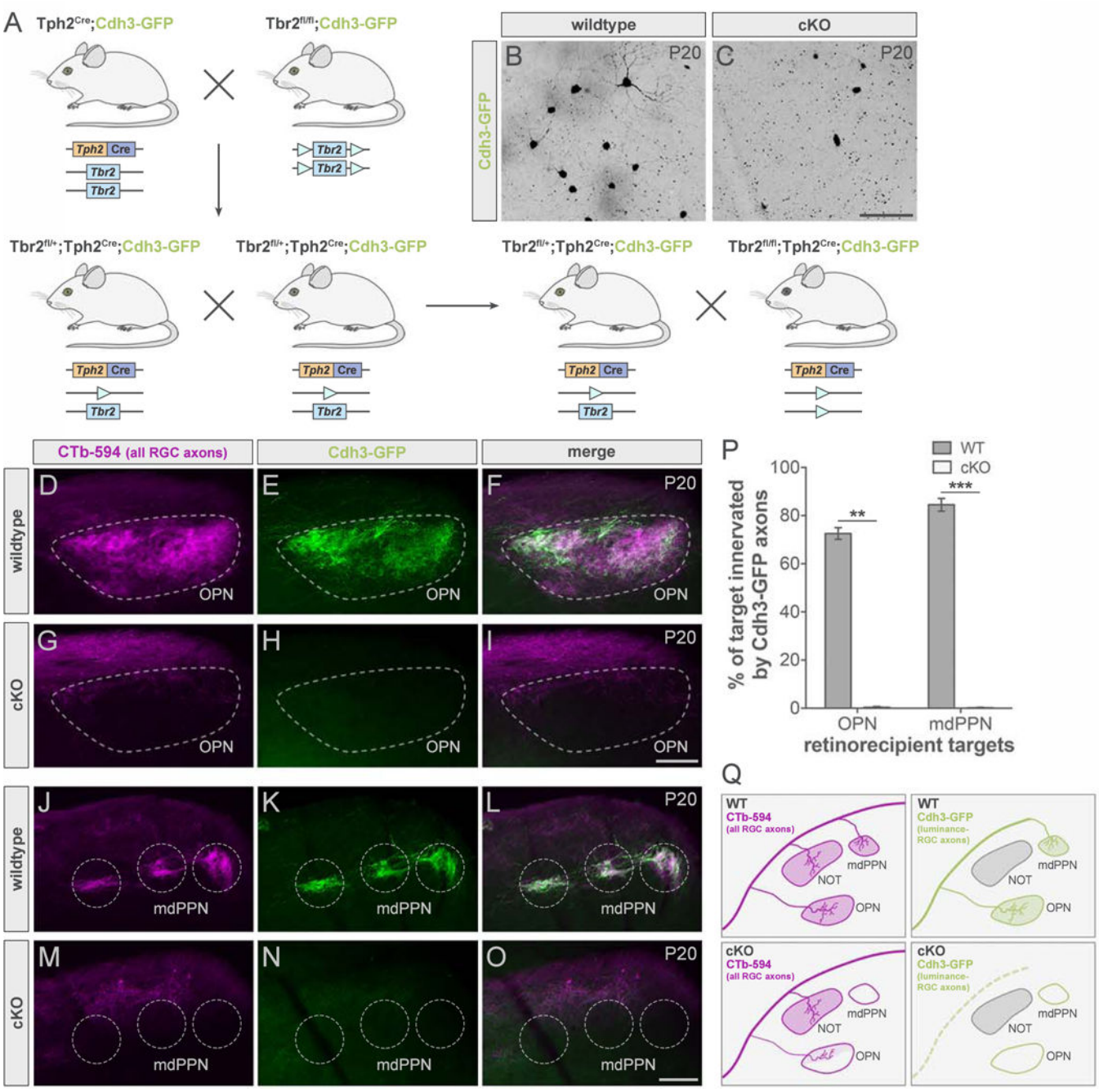

Figure 4. Conditional deletion of Tbr2 results in major loss of luminance-sensing RGCs and their axons

(A) Floxed Tbr2 strain crossed to the Tph2^{Cre} line to generate cKO mice (Tbr2$^{fl/fl}$;Tph2^{Cre}) mice and littermate controls (Tbr2$^{fl/+}$;Tph2^{Cre}; wildtype; WT). (B–C) Whole-mount retinas from WT (B) and cKO (C) mice with Cdh3-RGCs. Scale bar, 100 μm. (D–O) All RGC (CTb-594, magenta) and luminance-sensing RGC (Cdh3-GFP, green) axons in pretectum of WT (top panels) and cKO (bottom panels) mice. Scale bars, 100 μm. (P) Quantification of % of target innervated by Cdh3-GFP axons in WTs (dark gray) and cKOs (light gray). Data are represented as mean ± SEM (n = 3 mice per group); $^{**}p < 0.005$, $^{***}p < 0.001$, Student's *t*-

test. (Q) Summary schematic. mdPPN, medial division of the posterior pretectal nucleus; OPN, olivary pretectal nucleus. See also Figure S3.

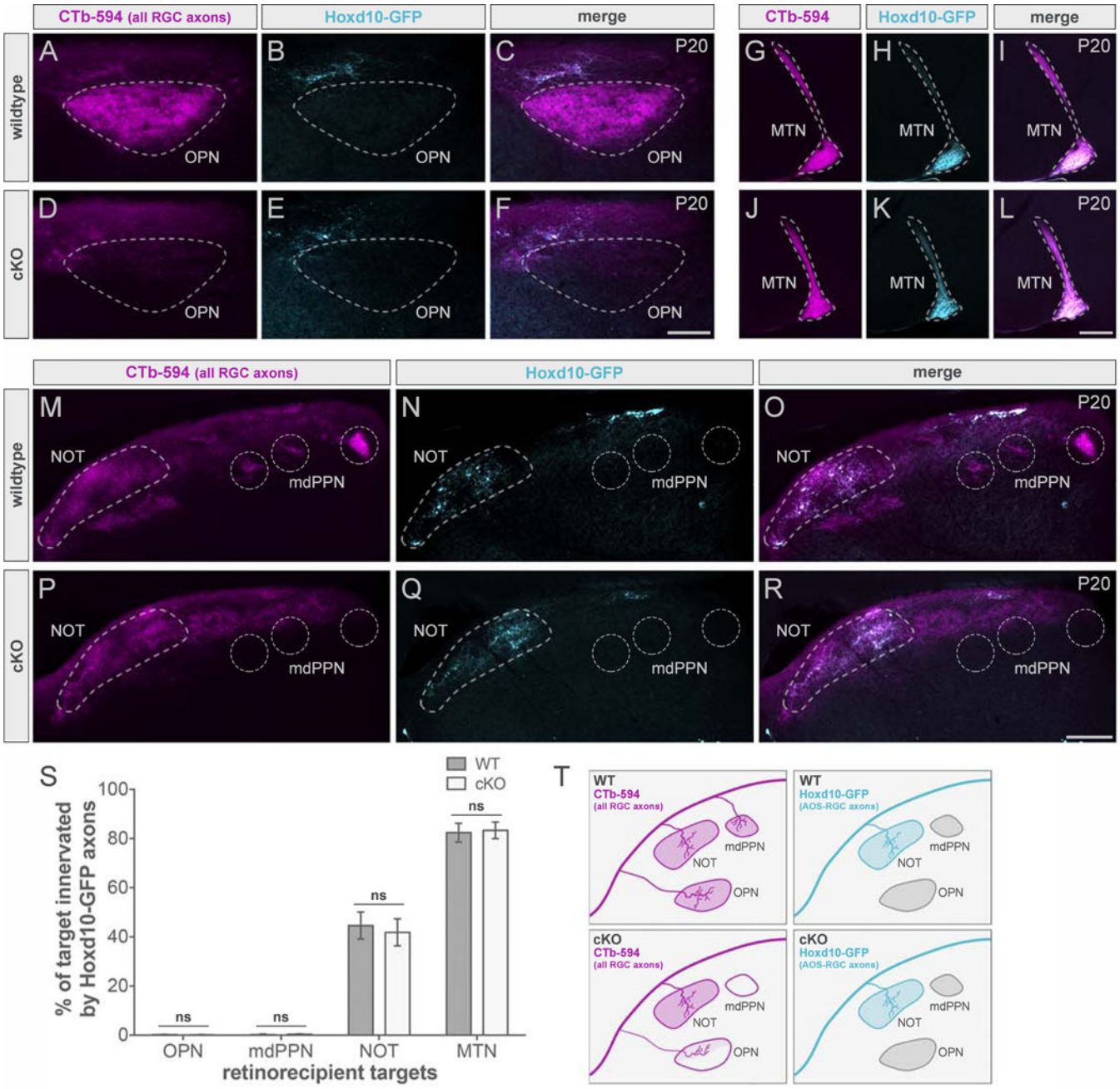

Figure 5. Eliminating one eye-to-brain pathway does not affect the innervation pattern of axons from other RGC types

(A–R) All RGC (CTb-594, magenta) and slow-DSGC (Hoxd10-GFP, cyan) axons in wildtype (WT; top panels) and cKO (bottom panels) mice. Scale bars, 100μm (A–F); 200μm (G–R). mdPPN, medial division of the posterior pretectal nucleus; MTN, medial terminal nucleus; NOT, nucleus of the optic tract; OPN, olivary pretectal nucleus. (S) Quantification of % of target innervated by Hoxd10-GFP axons in WT (dark gray) and cKO (light gray) mice. Data are represented as mean ± SEM (n = 3 mice per group); Student's *t*-test. (T) Summary schematic. See also Figures S4 and S5.

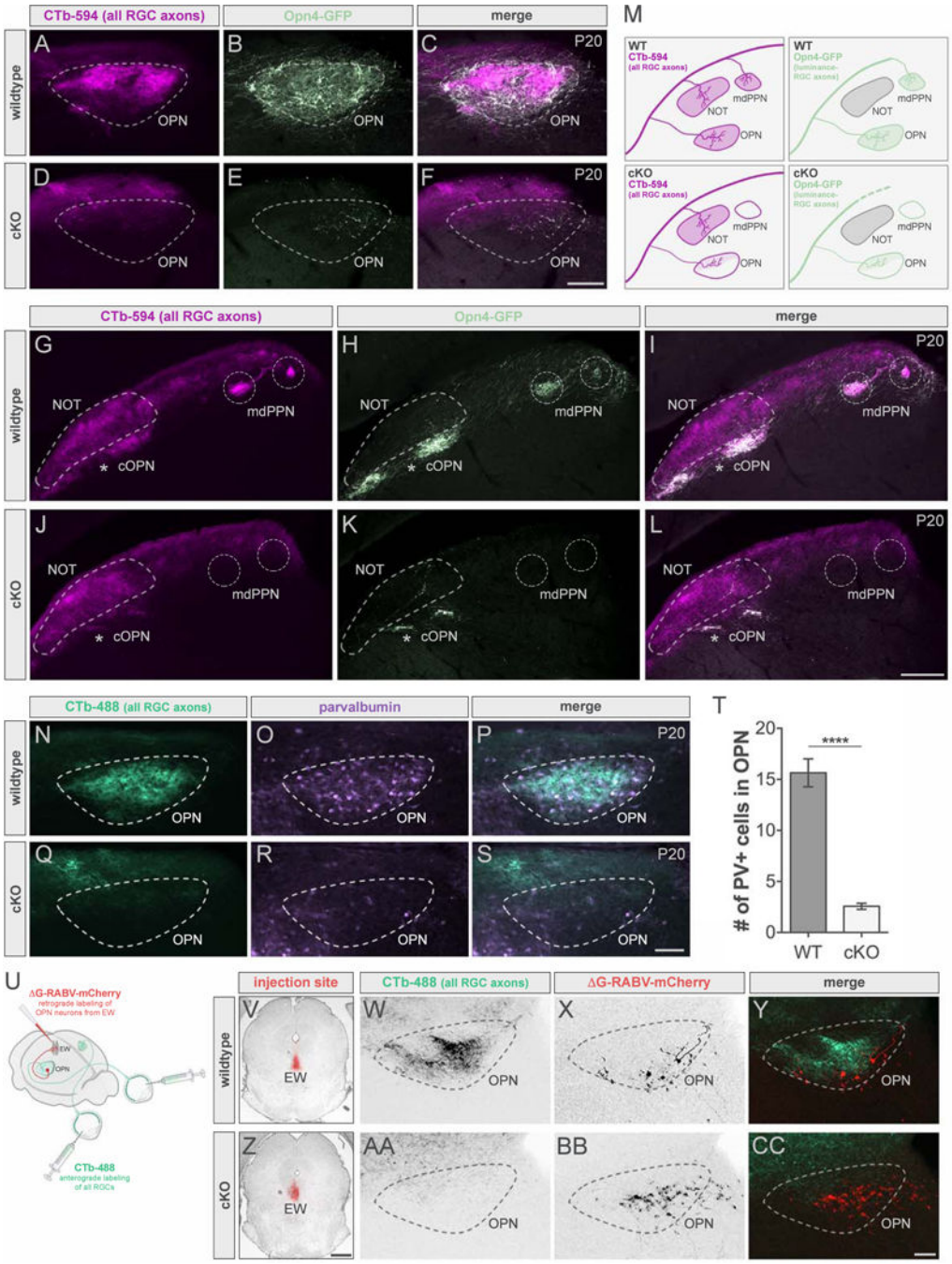

Figure 6. Poly-synaptic effects following ablation of most luminance-sensing RGCs

(A–L) All RGC (CTb-594, magenta) and luminance-sensing RGC (all ipRGCs, Opn4-GFP, light green) axons in wildtype (WT; top panels) and cKO (bottom panels) mice. Scale bars, 100μm (A–F); 200μm (G–L). (M) Summary schematic. See also Figure S6. (N–S) All RGC axons (CTb-488, green) and PV-expressing cells (purple) in WT (top panels) and cKO (bottom panels). Scale bar, 100μm. (T) Number of PV^+ cells in OPN of WTs (dark gray) and cKOs (light gray). Data are represented as mean ± SEM (n = 12-14 mice per group); ****$p < 0.0001$, Student's *t*-test. See also Figure S7. (U) Injection schematic. (V-CC) ΔG-RABV

injection site in WT (V) and cKO (Z) mice and corresponding sections of OPN showing all RGC axons (CTb-488, green) and cells retrogradely labeled from EW (red) in WT (W–Y) and cKO (AA–CC). cOPN, caudal OPN; EW, Edinger-Westphal nucleus; mdPPN, medial division of the posterior pretectal nucleus; NOT, nucleus of the optic tract; OPN, olivary pretectal nucleus. Scale bars, 100μm (W–Y and AA–CC); 800μm (V and Z).

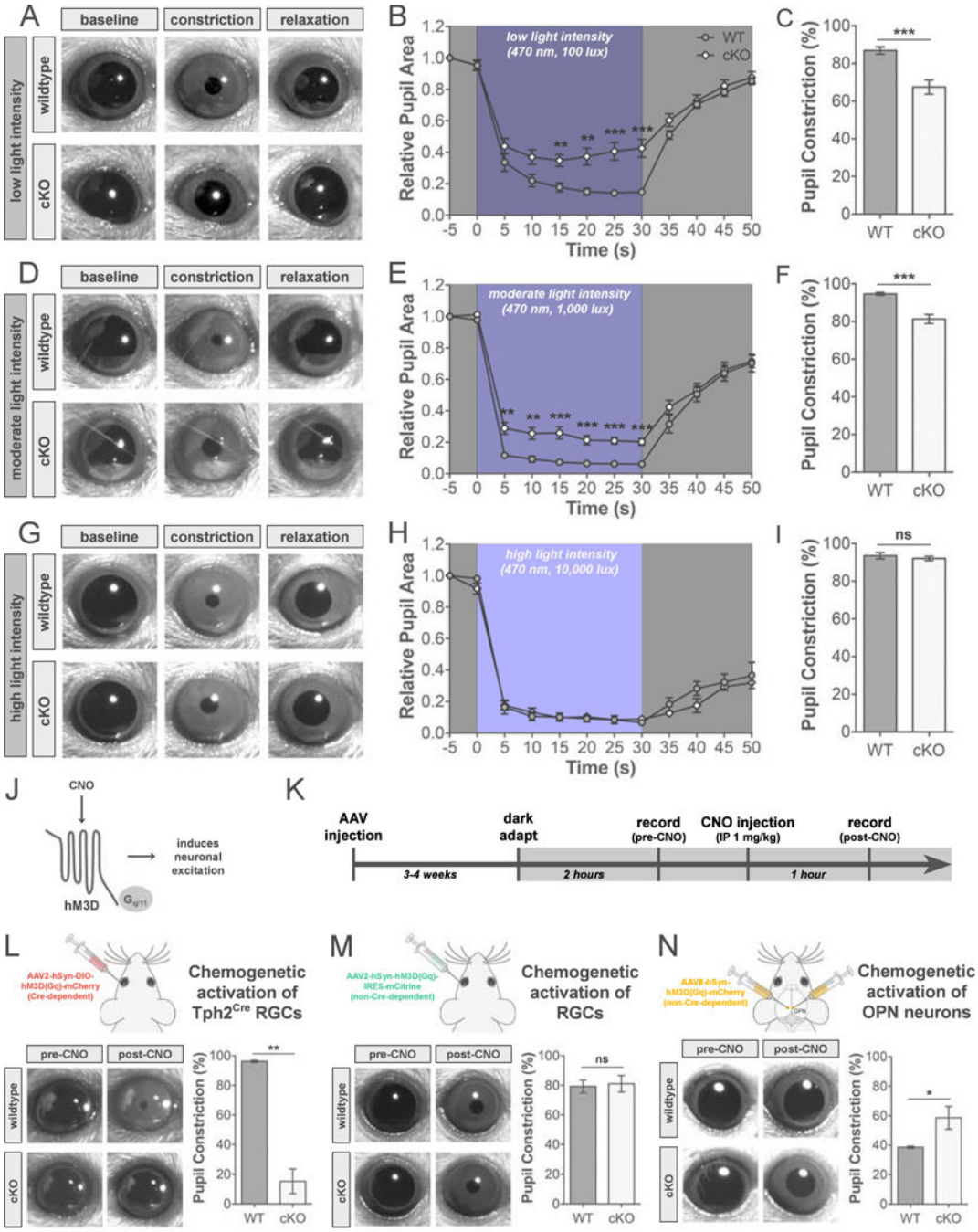

Figure 7. The effect of luminance-sensing RGC ablation on light- and chemogenetic-induced PLR

(A–I) PLR in response to a single blue LED at 100 (A–C), 1,000 (D–F), and 10,000 lux (G–I). (A, D, G) Examples of pupil size following dark adaptation, peak pupil constriction during light stimulation, and relaxed pupil size following light stimulation in wildtype (WT; top panels) and cKO (bottom panels) mice. (B, E, H) PLR time course in WT (dark gray) and cKO (light gray) mice plotted as pupil area relative to baseline pupil size. (C, F, I) Quantification of % of peak pupil constriction in WT (dark gray) and cKO (light gray) mice. Data are represented as mean ± SEM (n = 9–10 mice per group for B–C, E–F; 3–4 mice per

group for H-I); $^{**}p < 0.005$, $^{***}p < 0.001$, Student's *t*-test. (J) Diagram of G_q-coupled hM3D receptor. (K) Experimental timeline. (L–N) PLR analysis in response to chemogenetic activation of RGCs (L and M) or OPN neurons (N). Schematics of intravitreal or stereotaxic injections of hM3D viruses (top panels). Examples of pupil size before (pre-) and after (post-) CNO injection in WT and cKO mice (bottom left panels). Quantification of % of peak pupil constriction in WT (dark gray) and cKO (light gray) mice after injection of CNO (bottom right panels). Data are represented as mean ± SEM (n = 3–6 mice per group); $^{*}p < 0.05$, $^{**}p < 0.01$, Student's *t*-test. AAV, adeno-associated virus; CNO, clozapine-*N*-oxide; hM3D, human M3 muscarinic designer receptor; hSyn, human synaptophysin.